Progress In Electromagnetics Research, Vol. 124, 511–525, 2012

FREQUENCY-SELECTIVE NANOSTRUCTURED PLASMONIC ABSORBER BY HIGHLY LOSSY INTERFACE MODE

Y. Gong[1, 2, *], K. Li[1, 2], J. Huang[2], N. J. Copner[2], A. Davies[3], L. Wang[1], and T. Duan[1]

[1]State Key Laboratory of Transient Optics and Photonics, Xi'an Institute of Optics and Precision Mechanics, Chinese Academy of Sciences, Xi'an 710119, China

[2]Faculty of Advanced Technology, University of Glamorgan, CF37 1DL, UK

[3]Faculty of Health, Sport and Science, University of Glamorgan, CF37 1DL, UK

Abstract—We report on an existence of a highly lossy interface mode (HLIM) in a designed plasmonic nanostructure for perfect absorption of the incident optical waves. Interactions between the single thin-metallic-layer (TML) and slits arrays for excitation of the HLIM in the proposed plasmonic absorber are investigated, and eigenfrequency formula for the HLIM is derived. Analytical and numerical results show that the HLIM is frequency-selective, opens a narrow and steep absorption band in photonic stopband of the slits arrays. Due to the HLIM lossy characteristic, surface plasmon polaritons are significantly trapped at the TML interface with absorption close to 100%.

1. INTRODUCTION

Currently, the "bodies" with high absorption properties has played an important role in modern science and nanotechnologies for their useful applications such as thermal detectors [1, 2], nanoelectronic power sources [3], microbolometers [4], time-reversed lasers [5], and solar energy conversion [6, 7] The techniques to realize the high absorption attracts increasing attentions. It was shown that low-density vertically aligned carbon nanotube arrays can be engineered

Received 19 December 2011, Accepted 2 February 2012, Scheduled 13 February 2012

* Corresponding author: Yongkang Gong (gyk@opt.ac.cn).

to have an extremely low index of refraction, and the light wave impinging on it were totally absorbed [8]. Kravets et al. experimentally demonstrated that metal nanoparticles embedded in a dielectric matrix can strongly absorb light above 90% for a broad angle of incidence in visible-near infrared range [9]. Based on an anisotropic perfectly impedance-matched negative-index material, Avitzour et al. theoretically designed a wide-angle infrared perfect absorber with potential applications for infrared imaging and coherent thermal sources [10]. Another promising candidate to obtain high absorption is metamaterials which was first proposed in 2008 by Padilla's group who had demonstrated that perfect absorption was possible by properly engineering metamaterials' electric and magnetic responses to satisfy the impedance match [11]. Metamaterial absorber is a hot research topic nowadays, and various kinds of devices have emerged such as wide angle terahertz absorber [12, 13], millimeter-wave range absorber [14], polarization-insensitive absorber [15–17], wide-angle and polarization-independent absorber in optical frequency range [18], and dualband terahertz absorber [19–21].

An absorber with a broad or narrow bandwidth is both necessary in practical applications. The former can provide strong absorption of sunlight in entire solar bandwidth [22–24]. The latter has significant applications in selective thermal emitters [25, 26], all-optical switch [27], surface plasmon resonance sensor [28], and hyper spectral-single pixel imaging [29], etc.

In this paper, with excitation of a novel highly lossy interface mode (HLIM) by coupling a single thin-metallic-layer (TML) to slit arrays in a two-dimensional metal-dielectric-metal (MDM) nanostructure, we propose a frequency selective plasmonic absorber with tunable and narrow bandwidth. The paper is organized as follows. In Section 2, the plasmonic absorber structure is presented. Transmission matrix model to investigate its optical properties is established, and eigenfrequency formula for the HLIM is analytically derived. In Section 3, with transmission matrix method (TMM) and finite-difference time-domain (FDTD) method, optical spectra and field distributions for the plasmonic absorber are demonstrated, and characteristics of the HLIM are addressed. In Section 4, dependence of structure parameters on absorption spectra of the plasmonic absorber are investigated. The reflection dip depends very sensitively on the dielectric surrounding, generating a sensitivity of 1100 nm/RIU which is about two times higher than the recently reported nanostructured sensors based on metamaterials [30, 31], nanoparticles [32], and localized surface plasmon resonant [33] Finally, conclusions are made in Section 5.

2. STRUCTURE MODEL AND ANALYSIS METHOD

The plasmonic absorber understudy is schematically shown in Fig. 1. A two-dimensional MDM structure is composed of a dielectric core surrounded by two semi-infinite metallic claddings. A TML with thickness of L_m followed by slit arrays are inserted in the core. The width of the MDM core is w_1, and the distance between the TML to the first slit is L. There are N slits in the slit arrays, depth and width for each slit is D and w_2, respectively, and distance between each slit is L. The media at the left and right side of the TML are dielectrics A and B with refractive index of n_A and n_B, respectively. In our design, the metal is assumed to be gold whose permittivity can be characterized by Drude model of [25]

$$\varepsilon_m = 1 - \frac{\omega_p^2}{\omega^2 + i\omega\gamma}, \tag{1}$$

where $\omega_p = 1.37 \times 10^{16}$ rad/s and $\gamma = 1.22 \times 10^{14}$ rad/s are plasma frequency and damping constant, respectively. In the FDTD calculation, the waveguide mode source is emitted at the left waveguide. The structure reflection is $R = |S_{11}|^2$, transmission is $T = |S_{21}|^2$, and the absorption is $A = 1-R-T$. Here, the S_{11} and S_{21} are the reflection coefficient and transmission coefficient, respectively.

When a transverse magnetic polarized optical wave is illuminated

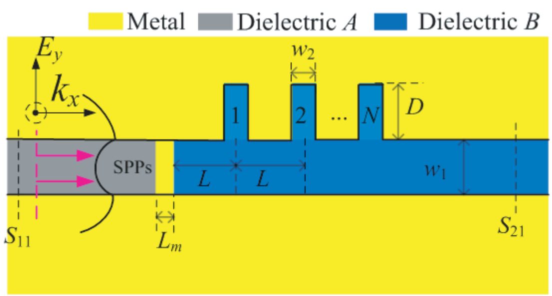

Figure 1. Schematic diagram of the proposed plasmonic absorber with a TML and slits arrays inserted in the core of a two-dimensional MDM structure. The yellow, cyan, and blue regions represent the metal, dielectric A, and dielectric B, respectively. The w_1, L_m, and L denote, respectively, width of the MDM core, thickness of the TML, and distance between the TML and the first slit. The distance between each slit is L, and there are N slits with each having a depth of D and width of w_2, respectively.

to the MDM structure, surface plasmon polaritons (SPPs) with relatively long propagation length and high confinement are excited [34], which can find wide applications such as nanolasers [35], waveguide [36, 37], all-angle negative refraction waveguides [38], nonlinear nanofocusing systems [39], etc.. In the structure shown in Fig. 1, the excited SPPs are confined to propagate in the dielectric A and travel to the TML. When the SPPs reach the TML, successively, they penetrate it and transmit to the dielectric B and the slit arrays. Aim to reveal how near-unity absorption is generated in above physical processes, we establish a transfer matrix model. At the left and right interfaces of the TML, the reflection and transmission occur with transfer matrixes of [40]

$$T_{l,r} = \tau_{l,r} \begin{pmatrix} 1 & \rho_{l,r} \\ \rho_{l,r} & 1 \end{pmatrix}, \tag{2}$$

where the T_l and T_r are transfer matrixes for the A/TML and TML/B interfaces, respectively. The $\tau_l = (n_l + n_m)/n_l/2$ and $\tau_r = (n_r + n_m)/n_m/2$, $\rho_l = (n_m - n_l)/(n_m + n_l)$, and $\rho_r = (n_r - n_m)/(n_r + n_m)$. Here, the n_l and n_r are effective refractive index of the SPPs propagating in the dielectrics A and B, respectively, and the n_m is the refractive index of the metal. The transfer matrixes for the SPPs propagating in the TML with length of L_m and the dielectric B with distance of L can be respectively described as

$$T_{TML} = \begin{pmatrix} e^{-ik_0 n_m L_m} & 0 \\ 0 & e^{ik_0 n_m L_m} \end{pmatrix}, \tag{3}$$

$$T_B = \begin{pmatrix} e^{-ik_0 n_r L} & 0 \\ 0 & e^{ik_0 n_r L} \end{pmatrix}. \tag{4}$$

Here, k_0 is propagation constant of optical wave in air.

Transmittance of the MDM waveguide coupled to a single slit can be described using the analogy between single-mode MDM waveguides and microwave transmission lines [41]. With this analogy, each slit in Fig. 1 is equivalent to an open-circuited transmission line with effective characteristic impedance described by $z_{slit} = z_s(z_L - iz_s \tan(\varphi))/(z_s - iz_L \tan(\varphi))$, where the $z_s = k_2 w_2/\varepsilon_0 \varepsilon_B \omega$, $z_L = (\varepsilon_B/\varepsilon_m)^{0.5} z_s$, and $\varphi = k_2 D$. Here, the k_2 is propagation constant of SPPs in the slit. With above simplified transmission-line model, the transfer matrix for each slit is expressed as [36]

$$T_{slit} = \begin{pmatrix} 1 + \dfrac{z_{slit}}{2z_{MDM}} & \dfrac{z_{slit}}{2z_{MDM}} \\ -\dfrac{z_{slit}}{2z_{MDM}} & 1 - \dfrac{z_{slit}}{2z_{MDM}} \end{pmatrix}. \tag{5}$$

Here, the $z_{MDM} = k_1 w_1/\varepsilon_0\varepsilon_B\omega$ is characteristic impedance of the MDM line, and the k_1 is propagation constant of SPPs in the MDM core.

With the Eqs. (1) to (5) described above, the total transfer matrix for the SPPs propagating along the TML and the slit arrays can be achieved as

$$T = T_l T_{TML} T_r (T_B T_{slit})^N = \begin{pmatrix} M_{11} & M_{12} \\ M_{21} & M_{22} \end{pmatrix}. \tag{6}$$

The Eq. (6) analytically gives us optical properties of the proposed structure. Its reflection coefficient, transmission coefficient, and absorption coefficient can be obtained as $r = M_{21}/M_{11}$, $t = 1/M_{11}$, and $A = 1 - |r|^2 - |t|^2$, respectively.

To guarantee the proposed structure with a high absorption, neither reflection nor transmission should happen. If we define that

$$T_2 \equiv (T_B T_{slit})^N = \begin{pmatrix} A_2 & B_2 \\ C_2 & D_2 \end{pmatrix}, \tag{7}$$

the structure reflection can be thereby expressed as

$$R = \left|\frac{M_{21}}{M_{11}}\right|^2 = \left|\frac{\left(\rho_l + \rho_r e^{i2k_0 n_m L_m}\right) A_2 + \left(\rho_l \rho_r + e^{i2k_0 n_m L_m}\right) C_2}{\left(1 + \rho_l \rho_r e^{i2k_0 n_m L_m}\right) A_2 + \left(\rho_r + \rho_l e^{i2k_0 n_m L_m}\right) C_2}\right|^2. \tag{8}$$

For the absorber, the numerator in Eq. (8) should be zero. Therefore, by applying some algebraic manipulations we can derive that

$$R_1 R_2 = 1, \tag{9}$$

where the $R_2 = |C_2/A_2|^2$ is reflection for the MDM structure with slit arrays are in the core (i.e., (i.e., the TML is not in the MDM structure shown in Fig. 1), and the R_1 is determined by $R_1 = |\rho_l\rho_r + \exp(i2k_0 n_m L_m)|^2/|\rho_l + \rho_r \exp(i2k_0 n_m L_m)|^2$. The eigenfrequency of Eq. (9) corresponds to an interface mode similar to the traditional optical Tamm states [42–44]. The difference is that optical Tamm sates are lossless, while the interface mode here is highly lossy.

Now we consider solution of Eq. (9). Provided that $L = 180\,\text{nm}$, $D = 200\,\text{nm}$ and $n_B = 1$, the R_2 versus frequency with different slit cell N is plotted in Fig. 2(a). Clearly, a photonic stopband is generated, where reflection reaches its maximum. However, due to the SPP losses it is smaller than 1. In order to realize Eq. (9), R_1 should be larger than 1. Variation of the R_1 to frequency at different L_m is shown in Fig. 2(b). It depicts that that R_1 increases with frequency, and especially, by adjusting L_m it can be tuned to be larger than 1. Above two characteristics enable us to satisfy Eq. (9) at a certain frequency locating in the photonic stopband by utilizing proper

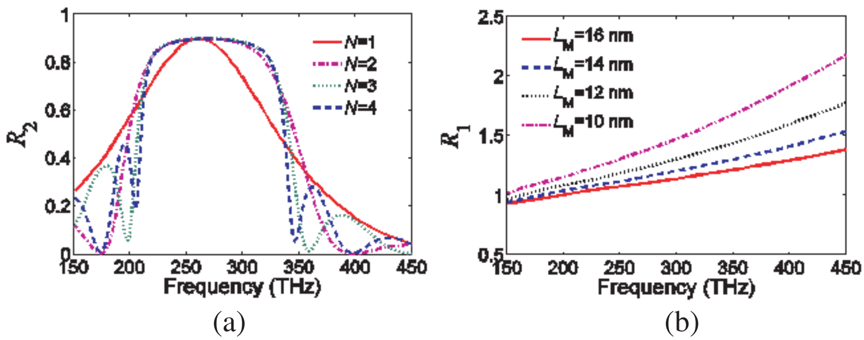

Figure 2. (a) R_2 versus frequency with different slit cell N. (b) Variation of R_1 to frequency and L_M. The other structure geometric parameters are: $L = 180\,\text{nm}$, $D = 200\,\text{nm}$, $w_1 = 60\,\text{nm}$, $w_2 = 60\,\text{nm}$, $n_A = 1$, and $n_B = 1$.

structure geometric parameters. In this case, no reflection occurs. Meanwhile, since the frequency is in the photonic stopband, there is no transmission either. As a result, perfect absorption happens here.

3. EXISTENCE OF THE HLIM AND SIMULATION RESULTS

Aim to show feasibility of the Eq. (9) for giving eigenfrequency of the proposed plasmonic absorber, the $R_1R_2 - 1$ versus frequency is calculated in Fig. 3(a) with $w_1 = 60\,\text{nm}$, $w_2 = 60\,\text{nm}$, $L_m = 14\,\text{nm}$, $L = 180\,\text{nm}$, $D = 200\,\text{nm}$, $N = 1$, $n_A = 1$, and $n_B = 1$. It is noted that the $R_1R_2 - 1$ reaches its minimum of zero at frequency of 261.4 THz. The red solid line in Fig. 3(a) shows the structure reflection spectrum analytically calculated by the Eq. (6). It demonstrates that a sharp zero dip appears at the position when $R_1R_2 - 1$ equals zero. The reflection spectrum is also numerically performed by FDTD method and depicted in Fig. 3(a) with blue circles. Obviously, the analytical results agree well with the FDTD results, which validate our TMM model for dealing with the proposed plasmonic absorber. The structure transmission (T) and absorption (A) spectra are calculated and plotted in Fig. 3(b). As predicted in the second section, the transmission is almost zero in the photonic stopband, and perfect absorption close to 100% is achieved at the frequency of the reflection dip. We can also observe that the plasmonic absorber possesses of absorption with steep band and narrow full-width at half-maximum (FWHM), which is attractive for sensing and imaging applications.

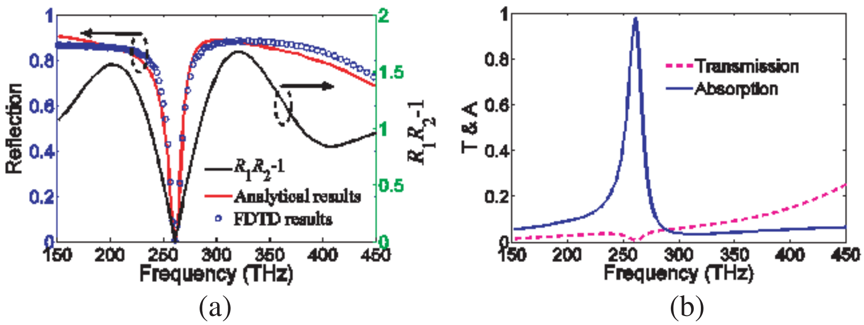

Figure 3. (a) Reflection spectrum of the plasmonic absorber and profile of the $R_1R_2 - 1$. The red solid line and blue circles represent the reflection obtained by the Eq. (6) and FDTD method, respectively. (b) Transmission and absorption spectra of the plasmonic absorber. The structure geometric parameters are: $L_m = 14\,\text{nm}$, $L = 180\,\text{nm}$, $D = 200\,\text{nm}$, $w_1 = 60\,\text{nm}$, $w_2 = 60\,\text{nm}$, $N = 1$, $n_A = 1$, and $n_B = 1$.

In order to reveal how TML interact with slit arrays to generate perfect absorption in the proposed plasmonic absorber, structure filed distributions are demonstrated by two-dimensional FDTD method. In the calculations, the perfect matching layers are set along x and y directions at edges of the structure. The spatial sizes are $\Delta x = \Delta y = 2\,\text{nm}$, and the temporal cell size is $\Delta t = \Delta x/(2c)$, where c is velocity of optical wave in vacuum. The source is continuous at eigenfrequency of 261.4 THz with amplitude of 1. Figs. 4(a) and (b) indicate that when the TML and slit are placed separately in the MDM structure, the SPPs are almost reflected. The former result arises from thickness of the TML approaching skin depth of the gold material, while the latter is due to the photonic stopband effect. When the slit is adjacent to the TML in the MDM structure as shown in Fig. 4(c), the Eq. (9) is satisfied, hence the SPPs pass through the TML without reflection. While the SPPs travel to the silt, they are reflected back to the TML and an interface mode is excited. Field amplitude of $|H_z|^2$ along $y = 0\,\mu\text{m}$ (i.e., the black dashed line in Fig. 4(c)) is plotted in Fig. 4(d), where the left and right perpendicular pink dotted line represent position of the TML/B interface and slit center, respectively. It demonstrates that the interface mode has a strong local-field enhancement at the TML/B interface. Due to metallic loss of the TML it is highly absorbed, decaying dramatically to zero at the A/TML interface and exponentially to zero at the slit center.

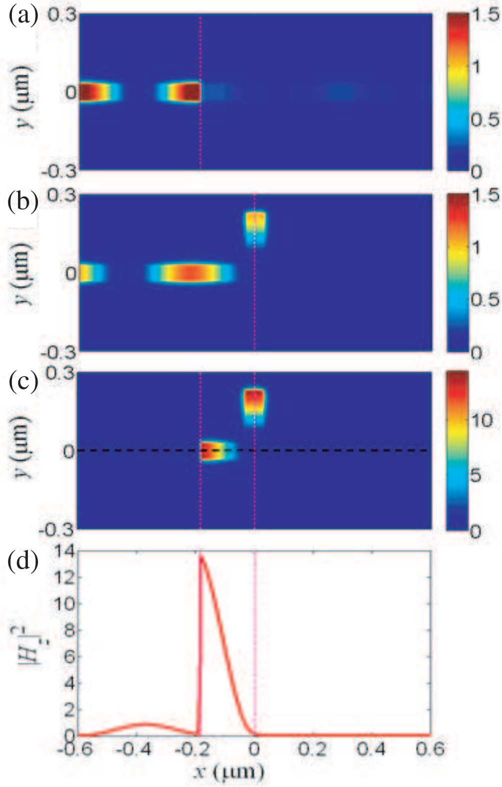

Figure 4. Field distributions of $|H_z|^2$ for the MDM structure at 261.4 THz with (a) single TML and (b) single slit in the MDM core. (c) The $|H_z|^2$ for the MDM structure at 261.4 THz when the TML and the slit are both inserted in the MDM core. The black dashed line illustrates $y = 0\,\mu\text{m}$. (c) The $|H_z|^2$ along the $y = 0\,\mu\text{m}$. Here, the left and right perpendicular pink dotted lines represent position of TML interface and slit center, respectively.

4. TUNABILITY OF THE PLASMONIC ABSORBER

In this section, tunability of the plasmonic absorber is investigated. As described in the Eq. (9), since the HLIM is frequency-selectively occurring in photonic stopband of the slit arrays, the absorption peak can be tuned by changing the structure geometric parameters to influence the photonic stopband. In our plasmonic absorber, the slit arrays with N cells can be assumed infinite periodic structures obey the Bloch-Floquet theorem. Each unit cell consists of a transmission line with length L and a susceptance. At the position of the nth unit cell, the column vector for the voltage fulfills

$$\hat{T}\begin{pmatrix} V_n^+ \\ V_n^- \end{pmatrix} = e^{\pm ik^{Bloch}L}\begin{pmatrix} V_n^+ \\ V_n^- \end{pmatrix}. \tag{10}$$

Here, V_n^+ and V_n^- are the forward and backward voltage in the nth unit cell, respectively, and k^{Bloch} is the Bloch-wave vector. The $\hat{T}$ is translation operator across single unit cell determined by

$$\hat{T} = T_B T_{slit} = \begin{pmatrix} e^{-ik_0 n_r L}\left(1+\frac{z_{slit}}{2z_{MDM}}\right) & e^{-ik_0 n_r L}\frac{z_{slit}}{2z_{MDM}} \\ -e^{ik_0 n_r L}\frac{z_{slit}}{2z_{MDM}} & e^{ik_0 n_r L}\left(1-\frac{z_{slit}}{2z_{MDM}}\right) \end{pmatrix}. \tag{11}$$

Therefore, the Bloch-wave dispersion relation for the slit arrays can be written as

$$\cos\left(k^{Bloch}L\right) = \frac{1}{2}(\hat{T}(1,1) + \hat{T}(2,2)). \tag{12}$$

When the magnitude of Eq. (12) is more than or equal to unity, the photonic stopband is generated. Dispersion curves of the $k^{Bloch}L/\pi$ versus the slit length L and depth D are plotted in Figs. 5(a) and (b), respectively. The black regions represent the photonic stopband of the slit arrays. Obviously, its position can be effectively tuned by varying L or D.

When $L_m = 14$ nm, $D = 200$ nm, $w_1 = 60$ nm, $w_2 = 60$ nm, $N = 3$, $n_A = 1$, and $n_B = 1$, the absorption spectra for the plasmonic absorber with $L = 130$, 180, and 230 nm are depicted in Fig. 6(a),

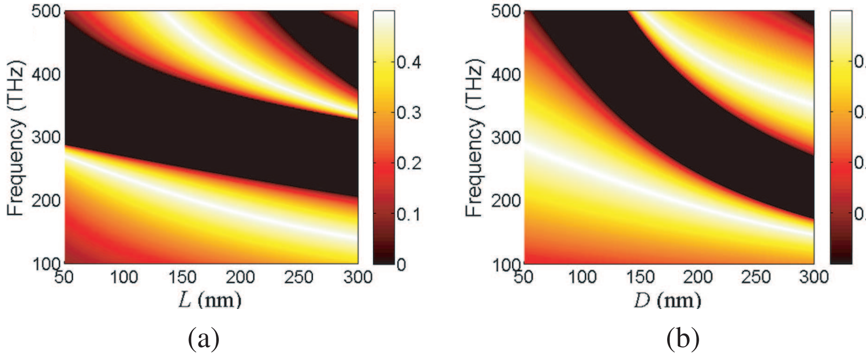

Figure 5. Dispersion for the SPPs propagating in slit arrays in MDM structure. (a) The $k^{Bloch}L/\pi$ versus frequency and L with $D = 200$ nm. (b) The $k^{Bloch}L/\pi$ versus frequency and D with $L = 180$ nm. The black region indicates the photonic stopband. The other structure geometric parameters are $w_1 = 60$ nm, $w_2 = 60$ nm, and $n_B = 1$.

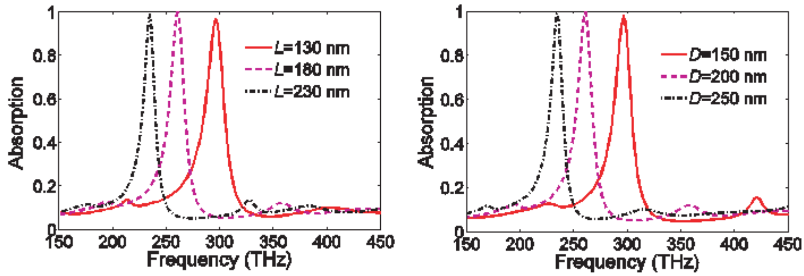

(a) (b)

Figure 6. Dependence of the absorption spectra on (a) L when $D = 200\,\text{nm}$ and (b) D when $L = 180\,\text{nm}$, respectively. The other structure geometric parameters are $L_m = 14\,\text{nm}$, $w_1 = 60\,\text{nm}$, $w_2 = 60\,\text{nm}$, $N = 3$, $n_A = 1$, and $n_B = 1$.

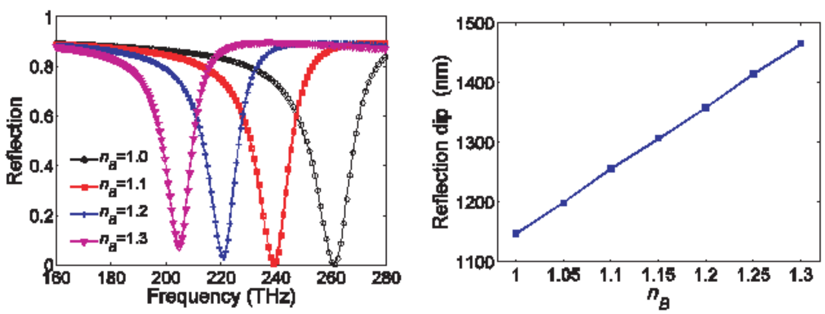

(a) (b)

Figure 7. (a) Reflection spectra of the plasmonic absorber with different dielectric B. (b) Refractive index n_B sensitivity to the reflection dip.

respectively. It shows that the absorption peak behaves a red-shift by increasing the L. A same phenomenon is also observed by increasing the D as shown in the Fig. 6(b), where the absorption spectra at $D = 150$, 200, and 250 nm with $L = 180\,\text{nm}$ are plotted, respectively. The physical reason for the redshift of the absorption peak can be easily understood from Fig. 6. Increasing L or D will vary the photonic stopband to the lower frequency and correspondingly, the HLIM will be shiftted to the lower frequency. Above results demonstrates that the proposed plasmonic absorber is highly flexible and its absorption peak can be effectively tuned by changing the structure size.

Dependence of the refractive index n_B on the reflection spectra of the plasmonic absorber is also studied as shown in Fig. 7(a). It is noteworthy that the position of the reflection dip can be substantially influenced by the materials in the plasmonic absorber When the n_B is changed from 1.0 to 1.1, 1.2, and 1.3, the reflection dip varies significantly from 261.4 to 238.9, 220.8, and 204.6 THz, respectively. This property can be well utilized for sensing applications. In Fig. 7(b), the wavelength of reflection dip versus the n_B is plotted, with a sensitivity (slop) about 1100 nm/RIU. This value is two times higher than the current nanosensors based on the metamaterials [30, 31], nanoparticles [32], and localized surface plasmon resonant [33] whose sensitivity is less than 500 nm/RIU. Therefore, the proposed plasmonic absorber can be used as an excellent sensing platform for chemical and biochemically relevant molecules such as live glucose [45] viruses [46], proteins, and DNA.

5. CONCLUSION

In conclusion, we have proposed and investigated a new kind of nanostructured plasmonic absorber based on the excitation of HLIM in a two-dimensional *MDM* structure. The transfer matrix model is established to analytically investigate the optical properties of the plasmonic absorber, which shows that the eigenfrequency of HLIM is frequency-selectively occurring in photonic stopband of the slits arrays with a narrow band response. The FDTD method is utilized to numerically study the field distributions of the plasmonic absorber. The results demonstrate that due to interaction between TML and slit arrays, the HLIM is excited at the TML interface with a strong local-field enhancement, and totally absorbed here because of the TML metallic losses. Dependence of structure geometric parameters on absorption spectrum is also investigated. It demonstrates that the absorption peak can be effectively tuned by varying L or D. Meanwhile, it depends very sensitively on the dielectric surrounding, yields sensitivity as high as 1100 nm/RIU. The proposed nanostructured plasmonic absorber possesses of a tunable and narrow absorption band, which may find potential applications such as in biomedical sensing, thermal emitting, and all-optical integrated photonic circuits.

ACKNOWLEDGMENT

This work was supported by the "Hundreds of Talents Programs" of the Chinese Academy of Sciences and by the National Natural Science Foundation of China under Grants 10874239, 10604066, 60907026, and

60537060. The authors acknowledge the fruitful discussions with Dr. Mingliang Ren, Dr. Wenfu Zhang, and Dr. Shaohui Yan.

REFERENCES

1. Parsons, A. D. and D. J. Pedder, "Thin-film infrared absorber structures for advanced thermal detectors," *J. Vac. Sci. Technol. A*, Vol. 6, 1686–1689, 1988.
2. Hayden, O., R. Agarwal, and C. M. Lieber, "Nanoscale avalanche photodiodes for highly sensitive and spatially resolved photon detection," *Nat. Mater.*, Vol. 5, 352–356, 2006.
3. Tian, B., X. Zheng, T. J. Kempa, Y. Fang, N. Yu, G. Yu, J. Huang, and C. M. Lieber, "Coaxial silicon nanowires as solar cells and nanoelectronic power sources," *Nature*, Vol. 449, 885–889, 2007.
4. Richards, P. L., "Bolometers for infrared and millimeter waves," *J. Appl. Phys.*, Vol. 76, No. 1, 1994.
5. Longhi, S., "Pi-symmetric laser absorber," *Phys. Rev. A*, Vol. 82, 031801, 2010.
6. Law, M., L. E. Greene, J. C. Johnson, R. Saykally, and P. D. Yang, "Nanowire dye-sensitized solar cells," *Nat. Mater.*, Vol. 4, 455–459, 2005.
7. Zukalova, M., A. Zukal, L. Kavan, M. K. Nazeeruddin, P. Liska, and M. Gratzel, "Organized mesoporous TiO_2 films exhibiting greatly enhanced performance in dye-sensitized solar cells," *Nano Lett.*, Vol. 5, 1789–1792, 2005.
8. Yang, Z. P., L. J. Ci, J. A. Bur, S. Y. Lin, and P. M. Ajayan, "Experimental Observation of an extremely dark material made by a low-density nanotube array," *Nano Lett.*, Vol. 8, 446, 2008.
9. Kravets, V. G., S. Neubeck, A. N. Grigorenko, and A. F. Kravets, "Plasmonic blackbody: Strong absorption of light by metal nanoparticles embedded in a dielectric matrix," *Phys. Rev. B*, Vol. 81, 165401, 2010.
10. Avitzour, Y., Y. A. Urzhumov, and G. Shvets, "Wide-angle infrared absorber based on a negative-index plasmonic metamaterial," *Phys. Rev. B*, Vol. 79, 045131, 2009.
11. Landy, N. I., S. Sajuyigbe, J. J. Mock, D. R. Smith, and W. J. Padilla, "Perfect metamaterial absorber," *Phys. Rev. Lett.*, Vol. 100, 207402, 2008.
12. Tao, H., C. M. Bingham, A. C. Strikwerda, D. Pilon, D. Shrekenhamer, N. I. Landy, K. Fan, X. Zhang, W. J. Padilla, and R. D. Averitt, "Highly flexible wide angle of incidence

terahertz metamaterial absorber: Design, fabricated and characterization," *Phys. Rev. B*, Vol. 78, 241103, 2008.
13. Kuznetsov, S. A., A. G. Paulish, A. V. Gelfand, P. A. Lazorskiy, and V. N. Fedorinin, "Matrix structure of metamaterial absorbers for multispectral terahertz imaging," *Progress In Electromagnetics Research*, Vol. 122, 93–103, 2012.
14. Cia, M. N., V. Torres Landivar, M. Beruete, and M. Sorolla Ayza, "A slow light fishnet-like absorber in the millimeter-wave range," *Progress In Electromagnetics Research*, Vol. 118, 287–301, 2011.
15. Wang, B., T. Koschny, and C. M. Soukoulis, "Wide-angle and polarization-independent chiral metamaterial absorber," *Phys. Rev. B*, Vol. 80, 033108, 2009.
16. Zhu, B., Z. Wang, C. Huang, Y. Feng, J. Zhao, and T. Jiang, "Polarization insensitive metamaterial absorber with wide incident angle," *Progress In Electromagnetics Research*, Vol. 101, 231–239, 2010.
17. Huang, L. and H. Chen, "Multi-band and polarization insensitive metamaterial absorber," *Progress In Electromagnetics Research*, Vol. 113, 103–110, 2011.
18. Hao, J. M., J. Wang, X. L. Liu, W. J. Padilla, L. Zhou, and M. Qiu, "High performance optical absorber based on a plasmonic metamaterial," *Appl. Phys. Lett.*, Vol. 96, 251104, 2010.
19. Wen, Q. Y., H. W. Zhang, Y. S. Xie, Q. H. Yang, and Y. L. Liu, "Dual band terahertz metamaterial absorber: Design, fabrication, and characterization," *Appl. Phys. Lett.*, Vol. 95, 241111, 2009.
20. Jiang, Z. H., S. Yun, F. Toor, D. H. Werner, and T. S. Mayer, "Conformal dual-band near-perfectly absorbing mid-infrared metamaterial coating," *ACS Nano.*, Vol. 5, 4641–4647, 2011.
21. He, X. J., Y. Wang, J. Wang, T. Gui, and Q. Wu, "Dual-band terahertz metamaterial absorber with polarization insensitivity and wide incident angle," *Progress In Electromagnetics Research*, Vol. 115, 381–397, 2011.
22. Rephaeli, E. and S. Fan, "Tungsten black absorber for solar light with wide angular operation range," *Appl. Phys. Lett.*, Vol. 92, 211107, 2008.
23. Yang, J., X. H. Hu, X. Li, Z. Liu, Z. X. Liang, X. Y. Jiang, and J. Zi, "Broadband absorption enhancement in anisotropic metamaterials by mirror reflections," *Phys. Rev. B*, Vol. 80, 125103, 2009.
24. Veronis, G., R. W. Dutton, and S. H. Fan, "Metallic photonic crystals with strong broadband absorption at optical frequencies

over wide angular range," *J. Appl. Phys.*, Vol. 97, 093104, 2005.

25. Sai, H. and H. Yugami, "Thermophotovoltaic generation with selective radiators based on tungsten surface gratings," *Appl. Phys. Lett.*, Vol. 85, 3399, 2004.
26. Liu, X. L., T. Tyler, T. Starr, A. F. Starr, N. M. Jokerst, and W. J. Padilla, "Taming the blackbody with infrared metamaterials as selective thermal emitters," *Phys. Rev. Lett.*, Vol. 107, 045901, 2011.
27. Gong, Y. K., Z. Y. Li, J. J. Fu, Y. H. Chen, G. X. Wang, H. Lu, L. R. Wang, and X. M. Liu, "Highly flexible all-optical metamaterial absorption switching assisted by Kerr-nonlinear effect," *Opt. Express*, Vol. 19, 10193–10198, 2011.
28. Liu, N., T. Weiss, M. Mesch, L. Langguth, U. Eigenthaler, M. Hirscher, C. Sönnichsen, and H. Giessen, "Infrared perfect absorber and its application as plasmonic sensor," *Nano Lett.*, Vol. 10, 2342–2348, 2010.
29. Liu, X. L., T. Starr, A. F. Starr, and W. J. Padilla, "Infrared spatial and frequency selective metamaterial with near-unity absorbance," *Phys. Rev. Lett.*, Vol. 104, 207403, 2010.
30. Liu, N., T. Weiss, M. Mesch, L. Langguth, U. Eigenthaler, M. Hirscher, C. Sonnichsen, and H. Giessen, "Planar metamaterial analogue of electromagnetically induced transparency for plasmonic sensing," *Nano Lett.*, Vol. 10, 1103–1107, 2010.
31. Xu, X., B. Peng, D. Li, J. Zhang, L. M. Wong, Q. Zhang, S. J. Wang, and Q. H. Xiong, "Flexible visible-infrared metamaterials and their applications in highly sensitive chemical and biological sensing," *Nano Lett.*, Vol. 11, 3232–3238, 2011.
32. Lal, S., S. Link, and N. J. Halas, "Nano-optics from sensing to waveguiding," *Nat. Photonics*, Vol. 1, 641–648, 2007.
33. Mayer, K. M. and J. H. Hafner, "Localized surface plasmon resonance sensors," *ACS Nano.*, Vol. 111, 3828–3857, 2011.
34. Dionne, J. A., L. A. Sweatlock, and H. A. Atwater, "Plasmon slot waveguides: Towards chip-scale propagation with subwavelength-scale localization," *Phys. Rev. B*, Vol. 73, 035407–035415, 2006.
35. Hill, M. T., M. Marell, E. S. P. Leong, B. Smalbrugge, Y. Zhu, M. H. Sun, P. J. van Veldhoven, E. J. Geluk, F. Karouta, Y. S. Oei, R. Nötzel, C. Z. Ning, and M. K. Smit, "Lasing in metal-insulator-metal sub-wavelength plasmonic waveguides," *Opt. Express*, Vol. 17, 11107–11112, 2009.
36. Gong, Y. K., L. R. Wang, X. H. Hu, X. H. Li, and X. M. Liu, "Broad-bandgap and low-sidelobe surface plasmon

polariton reflector with Bragg-grating-based MIM waveguide," *Optics Express*, Vol. 17, 13727–13736, 2009.

37. Neutens, P., P. V. Dorpe, I. D. Vlaminck, L. Lagae, and G. Borghs, "Electrical detection of confined gap plasmons in metal-insulator-metal waveguides," *Nat. Photonics*, Vol. 3, 283–286, 2009.
38. Shin, H. and S. Fan, "All-angle negative refraction for surface plasmon waves using a metal-dielectric-metal structure," *Phys. Rev. Lett.*, Vol. 96, 073907, 2006.
39. Davoyan, A. R., I. V. Shadrivov, A. A. Zharov, D. K. Gramotnev, and Y. S. Kivshar, "Nonlinear nanofocusing in tapered plasmonic waveguides," *Phys. Rev. Lett.*, Vol. 105, 116804, 2010.
40. Capmany, J., M. A. Muriel, and S. Sales, J. J. Rubio, and D. Pastor, "Microwave V-I transmission matrix formalism for the analysis of photonic circuits: Application to fiber bragg gratings," *J. Lightwave Technol.*, Vol. 21, 3125–3134, 2003.
41. Pannipitiya, A., I. D. Rukhlenko, and M. Premaratne, "Analytical modeling of resonant cavities for plasmonic-slot-waveguide junctions," *IEEE. J. Phot.*, Vol. 3, 220–233, 2011.
42. Shelykh, I. A., M. Kaliteevski, A. V. Kavokin, S. Brand, R. A. Abram, J. M. Chamberlain, and G. Malpuech, "Interface photonic states at the boundary between a metal and a dielectric Bragg mirror," *Phys. Stat. Sol. A*, Vol. 204, 522, 2007.
43. Vinogradov, A. P., A. V. Dorofeenko, S. G. Erokhin, M. Inoue, A. A. Lisyansky, A. M. Merzlikin, and A. B. Granovsky, "Surface state peculiarities in one-dimensional photonic crystal interfaces," *Phys. Rev. B*, Vol. 74, 045128, 2006.
44. Kavokin, A. V., I. A. Shelykh, and G. Malpuech, "Lossless interface modes at the boundary between two periodic dielectric structures," *Phys. Rev. B*, Vol. 72, 075127, 2005.
45. Kang, X., W. Tan, Z. Wang, and H. Chen, "Optic Tamm states: The Bloch-wave-expansion method," *Phys. Rev. A*, Vol. 79, 043832, 2009.
46. Yanik, A. A., M. Huang, O. Kamohara, A. Artar, T. W. Geisbert, J. H. Connor, and H. Altug, "An optofluidic nanoplasmonic biosensor for direct detection of live viruses from biological media," *Nano Lett.*, Vol. 10, 4962–4969, 2010.